Transactions of the Materials Research Society of Japan 25 [1] 209-212 (2000)

Synthesis and Electronic Properties of 2-Dimensional Quantum-Confined Titanium Oxide

Michitaka Ohtaki and Kozue Miyake
Department of Molecular and Material Sciences, Graduate School of Engineering Sciences, Kyushu University
6-1 Kasugakouen, Kasuga, Fukuoka 816-8580
Fax: +81-92-583-7465, e-mail: ohtaki@mm.kyushu-u.ac.jp

A lamellar mesophase of titanium oxide having a layered structure with a repeating length of *ca.* 35 Å was synthesized in the presence of cetyltrimethylammonium bromide surfactant as a molecular assembly template. The product showed only (*h*00) XRD peaks characteristic of lamellar mesophases, in which amorphous oxide layers and surfactant bilayers are alternately stacking. A hydrothermal post-treatment (HT) substantially sharpened the diffraction lines, while their positions remained the same. A Debye-Scherrer electron diffraction pattern observed only for the HT sample implied an improvement in crystallinity of the titanium oxide framework. Moreover, the HT sample showed a photocatalytic activity for oxidative decomposition of the surfactant under the light irradiation of 320 nm $\leq \lambda \leq$ 450 nm. Furthermore, a substantial blue shift of the band gap energy and a much steeper band edge strongly suggest confinement of electrons into a two-dimensional quantum structure.

Key words: mesoporous material, quantum size effect, titania, liquid crystal template, photocatalyst.

1. INTRODUCTION

A novel synthesis of MCM-41 mesoporous silica/silicate [1,2], whose chief characteristic is hexagonally aligned uniform cyrindrical channels with diameters of 30–100 Å, has triggered an extensive interest in inorganic mesophase formed by liquid crystal templating of surfactant micelles. Although the motivation of the synthesis of MCM-41 might have been development of extremely wide-bored zeolite catalysts, extraordinary catalytic activities have scarcely been reported on the MCM-41 family, and on their transition metal analogues as well. This may be due to the fact that the oxide framework of these mesoporous oxides has always been found amorphous so far [2,3].

Most of interests on MCM-41 and its related phases appear to focus on utilizing their well-controlled uniform channels. However, the dimension of the pore walls should also deserve wide scientific interest, because the observed thickness of the pore walls, typically about 10 Å, is far into a size region in which so-called quantum size effects become operative. Moreover, the highly anisotropic pore structures should provide the pore walls with a strong low-dimensionality. If a semiconducting material can form into the MCM-41–related structures, it may hence open a new insight in physics and chemistry of low-dimensional materials. Nevertheless, despite many intensive attempts to synthesize MCM-41 analogues with non-siliceous metal oxides [4-6], there has been no reports on emergence of semiconducting properties on the mesoporous oxides.

Titania (TiO_2) is a transition metal oxide, which is well known as oxide semiconductor as well as a white pigment. Photoelectrochemical applications of TiO_2 such as water splitting, wet photovoltaic cells, bactericidal and dirt-repellent effects have been extensively studied [7]. It would therefore be of great interest to synthesize MCM-41–like mesoporous materials with TiO_2. Nonetheless, successful synthesis of MCM-41 analogues with pure TiO_2 framework has scarcely been reported, while those with high Si/Ti ratios (» 10) like titanosilicate TS-1 can rather easily be obtained [8]. For instance, there has been an argument about the reproducibility of the first report on the synthesis of hexagonal mesophase of TiO_2 [9].

We have recently communicated for the first time on synthesis and photocatalytic activity of lamellar mesophase of titanium oxide, in which surfactant bilayer micelles and thin oxide layers are alternately stacking [10]. The activity as a semiconductor photocatalyst was observed only after hydrothermal post-treatment, and is hence expected to be a consequence of improved crystallinity of the TiO_2 sheet of *ca.* 10 Å thickness. Here we report low-temperature crystallization and the electronic properties of the thin TiO_2 layers of the lamellar phase.

2. EXPERIMENTAL

An aqueous solution of $TiCl_4$ prepared by adding dropwise $TiCl_4$ slowly into ice-cold distilled water was used as a Ti source. A strongly acidic clear solution was obtained. The Ti concentration of the solution was determined gravimetrically as *ca.* 1.0 mol/dm^3. Sodium dodecylphosphate ($C_{12}PO$) was used as a surfactant for the templating agent. On adding 50 cm^3 of the $TiCl_4$ solution into 50 cm^3 of 6 wt% aqueous solution of $C_{12}PO$, a white precipitate immediately formed. The mixture was then neutralized by adding ammonium hydroxide to bring the final pH to the desired values, and was kept overnight under moderate stirring. The white precipitate was collected by centrifuging, and was washed with distilled water for three times. A part of the as-prepared sample thus obtained was further subjected to a hydrothermal post-treatment (HT) with distilled water in a teflon-lined stainless steel autoclave. The products were finally dried at room temperature.

A powder X-ray diffraction (XRD) study of the products was carried out with a Rigaku RINT 1400 diffractometer using Cu Kα radiation. Transmission electron microscopy (TEM) was performed on a JEOL JEM-

2000FX transmission electron microscope operated at an acceleration voltage of 200 kV, at HREM Laboratory of Kyushu University.

Photocatalytic reactions were carried out in a closed-circulation reaction system under atmospheric conditions. A mixture of the TiO_2 sample and distilled water charged in a Pyrex reactor was irradiated with a 500 W xenon lamp, with inserting a cutoff optical filter into the light path when needed. Evolution of CO_2 in the gas phase was monitored by an in-line gas chromatograph. Diffuse-reflectance UV-vis spectra was collected on a JASCO UVDEC-660 spectrophotometer equipped with an integration sphere, and the spectra recorded in T% mode was converted into $F(R_\infty)$ by the Kubelka-Munk transform.

3. RESULTS AND DISCUSSION

The XRD patterns of as-synthesized products showed (h00) (h = 1,2,3) peaks which can be assigned to a lamellar structure with the d spacing of *ca.* 35 Å. The diffraction patterns are almost the same as that of the original silica/silicate counterpart, MCM-50. This is indicative that the products consist of alternately stacking $C_{12}PO$ bilayer micelles and thin titanium oxide sheets. The pH dependence of the XRD patterns and the d spacing of the as-prepared products is shown in Fig. 1. Optimal conditions obviously exist at around pH = 7, where the sharpest diffraction lines and the largest d spacing were observed. Diverging from this pH value, the XRD peaks broadened and the d spacing decreased. Although these results may be associated with the electrostatic interactions between TiO_2 precursors and the surfactant molecules, the details have not yet been clarified.

A hydrothermal (HT) post-treatment was further carried out to examine a possibility of low temperature crystallization of the lamellar TiO_2 sheets. As shown in Fig. 2, the XRD pattern of the as-prepared sample became more distinct after HT at 120 °C, while the peak positions remained the same. This result suggests an improvement in crystallinity or growth of a crystallographically coherent region. However, the diffraction lines broadened after HT at 150 °C with decreased d spacing, and finally disappeared after HT at 180 °C. The lamellar structure appears to collapse via HT at higher temperatures, probably due to thermal decomposition of the surfactant.

A TEM observation of the sample after HT at 120 °C revealed a well resolved lamellar structure with the oxide sheets of *ca.* 9 Å thickness as presented in Fig. 3, the alternating contrast of the layered structure being much clearer than those of the as-prepared samples. Whereas a selected area electron diffraction study yielded only diffuse halo patterns for the as-prepared samples, the sample after HT at 120 °C showed the Debye-Scherrer ring pattern consisting of many small bright dots, which pattern could be assigned to rutile-type TiO_2. These results strongly suggest crystallization of the thin TiO_2 sheets via HT. However, powder XRD measurements on the HT sample showed no peak in the higher angle region (2θ = 20 – 80°). This would be due to extremely small size of the TiO_2 sheet compared to the wavelength of the Cu $K\alpha$ radiation (λ = 1.54 Å), while the electron beam for TEM imaging appears to have a sufficiently short wavelength; an acceleration voltage of 200 keV corresponds to λ = 0.062 Å. Since the rutile-form of TiO_2 is a high-temperature phase while anatase is more stable at low temperature in bulk,

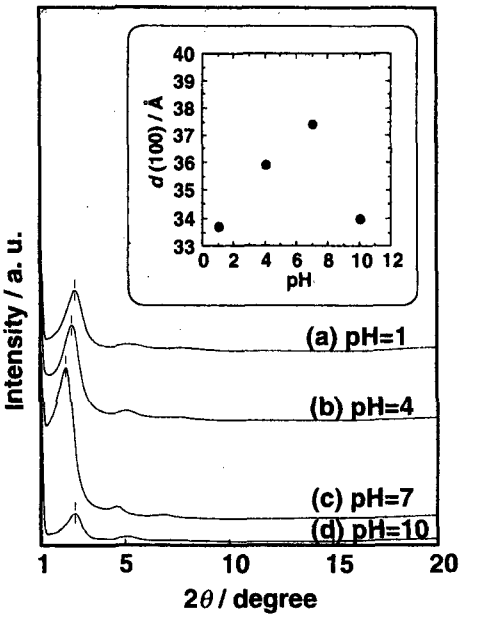

Fig. 1. XRD patterns of lamellar TiO_2 obtained from $TiCl_4$ aqueous solution at various final pH in the presence of $C_{12}PO$. The inset shows the d (100) spacings of the as-prepared products as a function of the final pH.

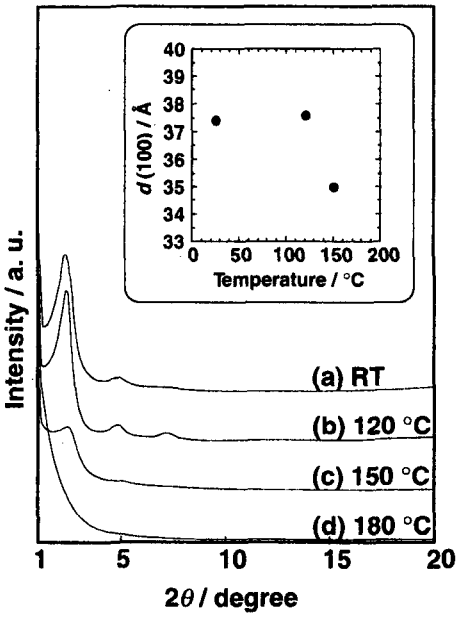

Fig. 2. XRD patterns of lamellar TiO_2 after hydrothermal post-treatment (HT) for 24 h at various temperature; (a) before HT, (b) HT at 120°C, (c) 150°C, and (d) 180°C. The inset shows the d (100) spacings of the products as a function of HT temperature.

preferential formation of the rutile-form rather than anatase at such low temperature seems to be anomalous. However, formation of rutile-type TiO_2 near room temperature has also been reported on syntheses of colloidal TiO_2 from $TiCl_4$ [11] or transparent TiO_2 sols [12,13]. Further study is necessary to discuss any relevance between the crystal form and the structure of the mesophase.

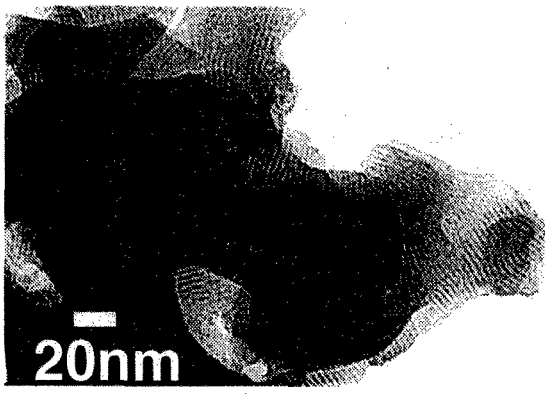

Fig. 3. TEM image of lamellar TiO_2 after hydrothermal post-treatment (HT) for 24 h at 120°C.

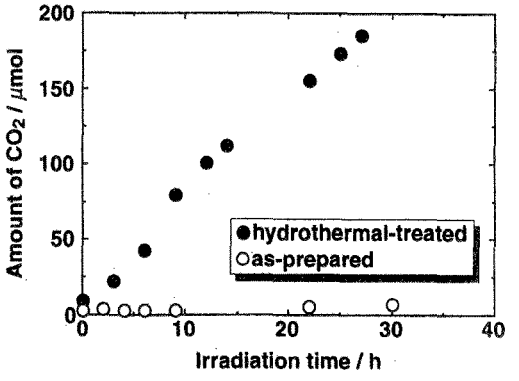

Fig. 4. The time courses of CO_2 evolution from lamellar titanium oxide before and after hydrothermal treatment at 120 °C. The samples were suspended in distilled water and irradiated with a 500W Xe lamp through a Pyrex glass reactor.

In order to examine emergence of a semiconducting nature of the TiO_2 sheets, photocatalytic activity of the samples suspended in distilled water was investigated. If the TiO_2 sheets can act as a semiconductor, interband photoexcitation will generate electron-hole pairs with a strong oxidizing power for degradation of organic compounds as having been proven for environmental applications of TiO_2. On irradiation with light of $\lambda \geq 250$ nm, no CO_2 evolution was detected for the as-synthesized sample, whereas a substantial CO_2 evolution was observed for the hydrothermal-treated sample as depicted in Fig. 4. The CO_2 evolution should be ascribed to oxidative decomposition of $C_{12}PO$, because the only C-containing species in the sample was $C_{12}PO$ constituting the bilayer templating micelles between the TiO_2 sheets.

Confirmation of the light-driven CO_2 generation was further carried out by changing the irradiation wavelength. Fig. 5 shows the wavelength dependence of the CO_2 evolution. The linear CO_2 evolution observed on full-band irradiation was completely prevented by cutting off the light of $\lambda \geq 450$ nm, and resumed on removing the cutoff filter from the light path. Shielding the light of $\lambda \geq 320$ nm from the irradiation, however, showed almost no influence on the CO_2 evolution. These results clearly indicate that the CO_2 evolution is caused by the light irradiation, and also reveal that a irradiation window of 320nm $\leq \lambda \leq 450$ nm is responsible for the CO_2 generation. Be-

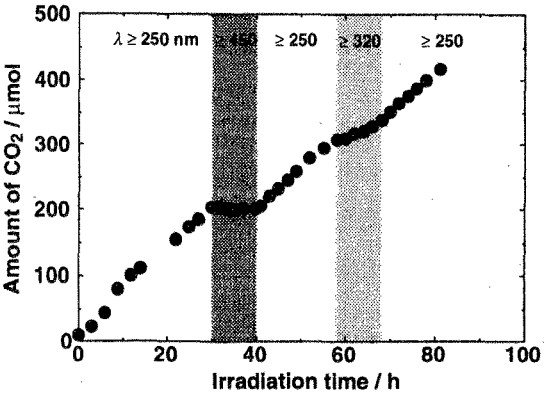

Fig. 5. The time course of CO_2 evolution from hydrothermal-treated lamellar titanium oxide with changing the irradiation cutoff wavelength. The sample was suspended in distilled water and irradiated with a 500W Xe lamp with inserting various cut-off filters into the light path.

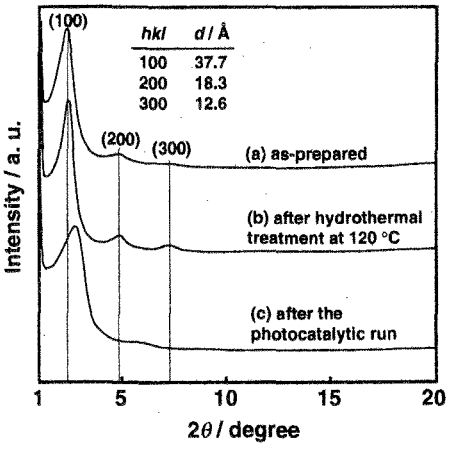

Fig. 6. XRD patterns of lamellar TiO_2; (a) as-prepared in the presence of $C_{12}PO$, (b) after hydrothermal treatment at 120 °C for 24 h, and (c) recovered after the photocatalytic run.

cause this window coincides with the absorption edge of crystalline TiO_2, these results are indicative of a semiconducting nature which the titanium oxide framework of the TiO_2 lamellar phase would have acquired. Moreover, this seems to be for the first time that the oxide framework of a oxide mesophase successfully crystallizes with retaining the highly ordered mesoporous structure.

The diffraction pattern of the lamellar TiO_2 after the photocatalytic reaction for 80 h broadened as shown in Fig. 6, the peak positions also shifting toward the lower angles (smaller d spacings). This would give another confirmation of that the origin of CO_2 was the surfactant molecules between the TiO_2 sheets, not those in the outer aqueous phase.

If the thin TiO_2 sheets become a semiconductor, a noticeable quantum size effect due to its very small thickness would occur. We have hence examined optical response of the samples by diffuse reflectance UV-vis spectroscopy in order to determine the band gap energy. Since the lowest absorption edge of rutile TiO_2 was reported to be assigned to the indirect transition [14], the Tauc plotting of $(\alpha h\nu)^{1/2}$ vs. $h\nu$ was applied as seen in Fig. 7. First

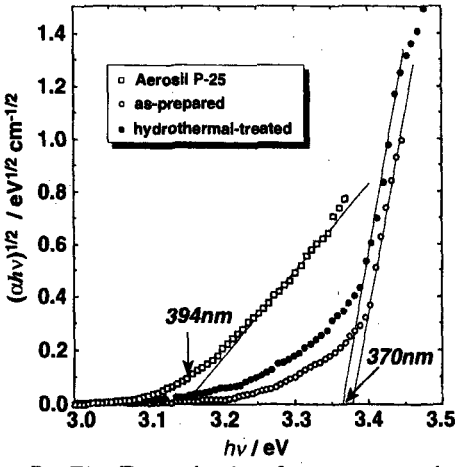

Fig. 7. The Tauc plotting for as-prepared and hydrothremal-treated lamellar TiO_2. Commercially obtained Aerosil P-25 is also shown as a reference for bulk crystalline TiO_2.

of all, the lamellar TiO_2 showed a substantial blue shift of the band gap energy from 394 nm (bulk TiO_2) to 370 nm (corresponding to a shift from 3.15 to 3.36 eV), evidencing strong confinement of electrons. According to Brus [15], the band gap shift ΔE_g in quantum-sized materials can be calculated by the following fomula;

$$\Delta E_g \approx \frac{h^2}{8R^2}\frac{1}{\mu} - \frac{1.8e^2}{\varepsilon R}$$

where R, radius of the particle; μ, reduced mass of the exciton, *i. e.*, $\mu^{-1} = m^*_e{}^{-1} + m^*_h{}^{-1}$, where m^*_e and m^*_h are the effective masses of electrons and holes, respectively; ε, dielectric constant of the material. Assuming $\mu = 2m_e$ and taking $\varepsilon = 184$ [12], one calculates $R = 0.9$ nm from the observed ΔE_g of 210 meV. This value strikingly matches with the observed thickness ($\approx 2R$) of the TiO_2 sheets as 9 Å, even taking into account that this calculation should be considered as only a first approximation.

Moreover, the slope of the band edge is much steeper for the lamellar TiO_2 than for bulk TiO_2. The sharp rise of the optical absorption may be a result of development of the band structure. However, theoretical consideration predicts that quantization of a parabolic band edge in 3D bulk crystal leads to a stairstep function in a 2D structure (one-dimensional quantum well) as depicted in Fig. 8. The two-dimensionality of the band structure might thereby account for the anomalously steep absorption edge of the lamellar TiO_2 shown in Fig. 7.

4. CONCLUSIONS

A lamellar titanium oxide mesophase was synthesized from $TiCl_4$ aqueous solution by using dodecylphosphate surfactant bilayer micelles as a structure-directing template. A hydrothermal post-treatment successfully crystallized the TiO_2 sheets of *ca.* 10 Å thickness, retaining its layered mesostructure. The crystallized lamellar TiO_2 sheets thus obtained were revealed to show a photocatalytic activity for oxidative photodegradation of the surfactant molecules intercalating between the sheets. The wavelength dependence of the CO_2 evolution clearly showed an active irradiation window of $320 \leq \lambda \leq 450$ nm, confirming emergence of the semiconducting nature via the crystallization of the TiO_2 framework.

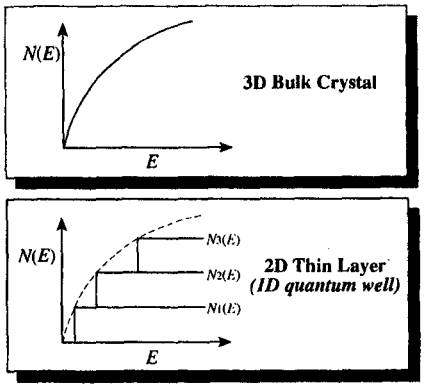

Fig. 8. Schematic of the density-of-states functions for 3D bulk crystal (assuming parabolic band) and for 2D thin layer (confinement in one direction).

A strong quantum size effect was suggested by a substantial blue shift of the absorption edge of the crystallized TiO_2 sheets at 3.36 eV (370 nm) compared to that of bulk crystalline TiO_2 at 394 nm. The markedly steep band edge implies two-dimensionality of the quantum confinement.

REFERENCES

[1] C. T. Kresge, M. E. Leonowicz, W. J. Roth, J. C. Vartuli, J. S. Beck, *Nature*, **359**, 710-712 (1992).

[2] J. S. Beck, J. C. Vartuli, W. J. Roth, M. E. Leonowicz, C. T. Kresge, K. D. Schmitt, C. T.-W. Chu, D. H. Olson, E. W. Sheppard, S. B. McCullen, J. B. Higgins, J. L. Schlenker, *J. Am. Chem. Soc.*, **114**, 10834-10843 (1992).

[3] C. Y. Chen, H. X. Li, M. E. Davis, *Microporous Mater.*, **2**, 17 (1993).

[4] Q. Huo, D. I. Margolese, U. Ciesla, D. G. Demuth, P. Feng, T. E. Gier, P. Sieger, A. Firouzi, B. F. Chmelka, F. Schüth, G. D. Stucky, *Chem. Mater.*, **6**, 1176-1191 (1994).

[5] Q. Huo, D. I. Margolese, U. Ciesla, P. Feng, T. E. Gier, P. Sieger, R. Leon, P. M. Petroff, F. Schüth, G. D. Stucky, *Nature*, **368**, 317-321 (1994).

[6] U. Ciesla, D. Demuth, R. Leon, P. Petroff, G. Stucky, K. Unger, F. Schüth, *J. Chem. Soc. Chem. Commun.*, **1994**, 1387-1388 (1994).

[7] A. L. Linsebigler, G. Lu, J. T. Yates, Jr., *Chem. Rev.*, **95**, 735-758 (1995).

[8] M. D. Alba, Z. Luan, J. Klinovski, *J. Phys. Chem.*, **100**, 2178-2182 (1996).

[9] D. M. Antonelli, J. Y. Ying, *Angew. Chem. Int. Ed. Engl.*, **34**, 2014-2017 (1995).

[10] H. Fujii, M. Ohtaki, K. Eguchi, *J. Am. Chem. Soc.*, **120**, 6832-6833 (1998).

[11] M. Ampo, T. Shima, S. Kodama, Y. Kubokawa, *J. Phys. Chem.*, **91**, 4305-4310 (1987).

[12] C. Kormann, D. W. Bahnemann, M. R. Hoffmann, *J. Phys. Chem.*, **92**, 5196-5201 (1988).

[13] H. Yoneyama, S. Haga, S. Yamanaka, *J. Phys. Chem.*, **93**, 4833-4837 (1989).

[14] K. Vos, *J. Phys. C*, **10**, 3917-3939 (1977).

[15] L. E. Brus, *J. Phys. Chem.*, **90**, 2555 (1986).

(Received December 16,1999 ; Accepted January 31,2000)